Received: 8 November 2019 | Revised: 4 July 2021 | Accepted: 30 August 2021

DOI: 10.1111/jnc.15505

Journal of Neurochemistry JNC The Official Journal of the International Society for Neurochemistry WILEY

ORIGINAL ARTICLE

Transient expansion of the expression region of *Hsd11b1*, encoding 11β-hydroxysteroid dehydrogenase type 1, in the developing mouse neocortex

Miyuki Doi[1] | Yuichiro Oka[1,2] | Manabu Taniguchi[1] | Makoto Sato[1,2,3]

[1]Department of Anatomy and Neuroscience, Graduate School of Medicine, Osaka University, Suita, Osaka, Japan

[2]Molecular Brain Science, Division of Developmental Neuroscience, Department of Child Development, United Graduate School of Child Development, Osaka University, Kanazawa University, Hamamatsu University School of Medicine, Chiba University, and University of Fukui (UGSCD), Osaka University, Suita, Osaka, Japan

[3]Graduate School of Frontier Biosciences, Osaka University, Suita, Osaka, Japan

Correspondence
Makoto Sato, Department of Anatomy and Neuroscience, Graduate School of Medicine, Osaka University, Suita, Osaka, Japan.
Email: makosato@anat2.med.osaka-u.ac.jp

Funding information
Takeda Science Foundation; KAKENHI, Grant/Award Number: 20H03414, JP15K15015, JP17H04014, JP17K07076, JP25293043 and JP26830027; Naito Foundation; NOVARTIS Foundation (Japan) for the Promotion of Science

Abstract

Corticosteroids are stress-related hormones that maintain homeostasis. The most effective corticosteroids are corticosterone (CORT) in rodents and cortisol in primates. 11β-Hydroxysteroid dehydrogenase type 1 (11β-HSD1; EC 1.1.1.146), encoded by *Hsd11b1*, is a key regulator of the local concentration of CORT/cortisol. *Hsd11b1* expression in layer 5 of the primary somatosensory cortex has been shown in adult mice. However, its localization in the entire neocortex, especially during development, has not been fully addressed. Here, we established robust and dynamic expression profiles of *Hsd11b1* in the developing mouse neocortex. *Hsd11b1* was found mostly in pyramidal neurons. By retrograde tracing, we observed that some *Hsd11b1*-positive cells were projection neurons, indicating that at least some were excitatory. At postnatal day 0 (P0), *Hsd11b1* was expressed in the deep layer of the somatosensory cortex. Then, from P3 to P8, the expression area expanded broadly; it was observed in layers 4 and 5, spanning the whole neocortex, including the primary motor cortex (M1) and the primary visual cortex (V1). The positive region gradually narrowed from P14 onwards and was ultimately limited to layer 5 of the somatosensory cortex at P26 and later. Furthermore, we administered CORT to nursing dams to increase the systemic CORT level of their pups. Here, we observed a reduced number of *Hsd11b1*-positive cells in the neocortex of these pups. Our observation suggests that *Hsd11b1* expression in the developing neocortex is affected by systemic CORT levels. It is possible that stress on mothers influences the neocortical development of their children.

KEYWORDS
cortex, corticosterone, cortisol, development, mother–child relationship, stress

Abbreviations: 11β-HSD1, 11β-hydroxysteroid dehydrogenase type1; A1, primary auditory cortex; Cg, cingulate cortex; CORT, corticosterone; CPu, caudate putamen; cS1, contralateral primary somatosensory cortex; ctip2, chicken ovalbumin upstream promoter transcription factor-interacting proteins 2; Cux1, cut-like homeobox 1; DAPI, 4′,6-diamidino-2-phenylindole; DDW, double distilled water; FG, FluoroGold; GR, glucocorticoid receptor; GRE, glucocorticoid-responsive element; hippo, hippocampus; IHC, immunohistochemistry; ISH, *in situ* hybridization; LTP, long-term potentiation; M1, primary motor cortex; M2, secondary motor cortex; mPFC, medial prefrontal cortex; MR, mineralocorticoid receptor; NBT/BCIP, nitro blue tetrazolium chloride/5-bromo-4-chloro-3-indolyl-phosphate; P, postnatal day; PBS, phosphate-buffered saline; PCR, polymerase chain reaction; PFA, paraformaldehyde; PtA, parietal association cortex; ROI, region of interest; RS, retrosplenial cortex; RT, room temperature; SEM, standard error of mean; S1, primary somatosensory cortex; S2, secondary somatosensory cortex; SSC, saline sodium citrate; V1, primary visual cortex.

1 | INTRODUCTION

Corticosteroids play an important role in the maintenance of homeostasis. The most effective corticosteroids are corticosterone (CORT) in rodents and cortisol in primates (Scorrano et al., 2015). Their local concentrations are controlled by 11β-HSD1, encoded by *Hsd11b1*, which converts inactive 11-dehydrocorticosterone and cortisone into active CORT and cortisol, respectively (Sandeep & Walker, 2001; Seckl, 1997). Whereas this enzyme works inside cells, CORT and cortisol are capable of functioning outside cells owing to their lipid permeability (Andrew et al., 2005; Yau et al., 2007).

Hsd11b1 is expressed in various tissues, including the brain. 11β-HSD1 regulates CORT levels in the hippocampus (Holmes et al., 2010). Two different types of receptors for CORT/cortisol, mineralocorticoid receptor (MR) and glucocorticoid receptor (GR), have been reported (Funder 1997). The MRs are occupied and predominantly activated by a low level of CORT, whereas the GRs, in addition to MRs, are occupied and activated by a high level of CORT (Chapman et al., 2013). More interestingly, a low level of CORT, apparently via MRs, leads to enhanced long-term potentiation (LTP), whereas a high level of CORT, seemingly via both MRs and GRs, results in contrasting effects and a decrease in LTP (Diamond et al., 1992). Furthermore, corticosteroids suppress microglial proliferation. GR-mediated microglial activation and dendritic spine plasticity have also been reported (Moda-Sava et al., 2019; Pedrazzoli et al., 2019).

Although the underlying mechanisms are not fully elucidated, it is likely that CORT/cortisol plays an important role in brain development. Strong stress due to maternal separation reduces the number of spines of a neuron and induces hypersensitivity to somatosensory stimulation, as evaluated by the von Frey hair test in the mouse (Takatsuru et al., 2009). It has been shown that the blood level of CORT is elevated by stress and that a high blood level of CORT during the suckling period leads to cognitive impairment (Macrì et al., 2009). Clinically, it is suggested that there is a relationship between the childhood blood cortisol level and the strength of amygdala-mPFC connectivity, which is related to emotion (Burghy et al., 2012). Therefore, the level of CORT/cortisol *in situ* must be precisely controlled during brain development.

Although the involvement of 11β-HSD1 is assumed to be related to the local concentration of CORT/cortisol, when and where 11β-HSD1 works have not been fully understood. Here, focusing on the neocortex, we examined the temporal and spatial expression of *Hsd11b1*, especially during development. Furthermore, we specifically asked how *Hsd11b1* expression was regulated. Unexpectedly, robust and dynamic developmental profiles of *Hsd11b1* were observed. More importantly, our results suggest specific crosstalk between systemic CORT and local *Hsd11b1* expression.

2 | MATERIALS AND METHODS

This study was not pre-registered.

2.1 | Animals

In this study, wild-type male ICR mice were purchased from SLC Japan (Cat#5652524, RRID: MGI:5652524). Mice were able to access food and water freely. They were housed under a 12-h light/dark cycle. Postnatal day 0 (P0) was defined as the date of birth. All animal procedures were approved by the Animal Experimentation Committee of Osaka University and were performed in accordance with the Regulation on Animal Experimentation at Osaka University (approval reference number: 30-061-012) and the ARRIVE guidelines. In this study, we used a combination anesthetic (MMB: 0.3 mg/kg medetomidine, 4.0 mg/kg midazolam, and 5.0 mg/kg butorphanol) and hypothermia to minimize animal suffering. We chose MMB in accordance with the anesthesia guidelines issued by the Animal Experimentation Committee of Osaka University. The total number of mice used in this study was 63. To examine the distribution pattern of *Hsd11b1*-positive cells in the developmental cortex, we used 27 mice. For retrograde tracing, we used three mice. In the whisker ablation experiment, we used three mice. In the CORT administration experiment (P21-P31), we used three mice per group. In the CORT administration experiment (P1-P11), we used 12 mice per group to measure the blood concentration of CORT and analyzed six mice per group. After surgery, the operated animals did not show any pain-related behaviors, such as twisting their body and/or decreasing in appetite. Therefore, we did not apply pain medication after the surgery. In anesthesia and post-operative care, we followed the recommendation by the Institute of Experimental Animal Sciences Faculty of Medicine, Osaka University.

2.2 | Retrograde tracing

Mice were anesthetized with MMB by intraperitoneal injection and fixed on the stereotaxic frame. Then, the skull was opened. Four percent FG (Cat#52-9400, Fluorochrome, Inc) in DDW containing 1 mg/mL Fast Green (Cat#F7258-25G, Sigma-Aldrich) was injected into cS1 (1.5 mm posterior to bregma, 3.0 mm lateral, 0.5 mm below the surface), (1.0, 3.0, 0.5), (0.5, 3.0, 0.5), (0.0, 3.0, 0.5) or M1 (0.7 mm anterior to bregma, 1.0 mm lateral, 0.75 mm below the surface), (1.2, 1.2, 0.75), (1.5, 1.5, 0.75) with a glass pipette connected with a Hamilton syringe (Cat#4015-21011, Hamilton Company). The scalp was sutured after injection. After 5 days, mice were anesthetized with MMB and transcardially perfused with cooled phosphate-buffered saline (PBS) followed by 4% paraformaldehyde (PFA) in PBS. No exclusion criteria were predetermined, and no animals were excluded. We performed tracer injection in the afternoon (13:00–20:00).

2.3 | Tissue processing

Mice (P0, P3, P4, P6, P8, P14, P17, P26, P56) were anesthetized with MMB by intraperitoneal injection and transcardially perfused with

cooled PBS and then with 4% PFA in PBS. Brains were dissected out and fixed in 4% PFA in PBS for 24 h at 4°C and then cryoprotected in 30% sucrose in PBS for 48 h at 4°C. Brains were embedded in O.C.T. Compound (Cat#45833, SFJ) and then sliced into 16-μm coronal sections using a cryostat (Leica, CM3050S, RRID: SCR_016844). Sections were thaw mounted on SuperFrost glass slides (Cat#S2443, Matsunami) and kept in freezer at −80°C.

2.4 | Probe generation

cDNA fragments of *Hsd11b1* were amplified with PCR using mouse brain cDNA as a template and the following primer pair: *Hsd11b1*-Fw: 5′ CCAGGGAAAGAAAGTGATTGTC 3′ and *Hsd11b1*-Rv: 5′ GTTCTAAGACCACTCACCAGGG 3′. The amplified fragment was cloned into the pGEM-T vector (Cat#A3600, Promega) and digested with *Nco*I for linearization. The sequence of the amplified fragment was confirmed by Sanger sequencing. *In vitro* transcription was performed with SP6 RNA polymerase (Cat#10810274001, Roche) using linearized template and DIG RNA labeling mix (Cat#11277073910, Roche) according to the manufacturer's instructions.

2.5 | *In situ* hybridization

Sections were air-dried for 1 h and then fixed in 4% PFA for 10 min. After the endogenous alkaline phosphatases were inactivated in 0.2 M HCl for 10 min, the sections were permeabilized with proteinase K (3.85 μg/mL; Cat#03115828001, Roche) at 37°C (P0, P3, 3 min; P4, P6, 4 min; P8, P14, 5 min; and P26, 10 min). Next, sections were acetylated with acetic anhydride in 0.1 M triethanolamine (pH 8.0) for 10 min and equilibrated with 5× SSC for more than 10 min. Sections were rinsed with PBS for 5 min in between steps. Finally, the sections were hybridized with the *Hsd11b1* probe in hybridization buffer (50% formamide, 5× SSC, 0.1 mg/mL Baker's yeast tRNA; Cat#10109495001, Roche) for 16 h at 55°C. The next day, sections were washed in the following steps: 5× SSC, 20 min at room temperature (RT, 22-24°C); 2× SSC, 20 min at 65°C; 0.2 × SSC, 20 min at 65°C; 0.2 × SSC, 20 min at 65°C. After a rinse in PBS, the sections were treated with blocking buffer (1% blocking reagent in PBS; Cat#11096176001, Roche) for 1 h at RT. Then, the sections were reacted with anti-DIG coupled with alkaline phosphatase (Fab fragment) (Cat#1109274910, Roche) (1:1000 dilution in blocking buffer) for 2 h at RT. Finally, the signals were detected using nitro blue tetrazolium chloride/5-bromo-4-chloro-3-indolyl-phosphate (NBT/BCIP; Cat#1138312301, Cat#11383221001, Roche). Sections were mounted with Fluoromount^{TM} (Cat#K 024, Diagnostic BioSystems) and kept at 4°C until microscopic observation.

2.6 | Immunohistochemistry (IHC)

The primary antibodies used in this study were as follows: anti-Ctip2 (1:400; rat; Cat#ab18465, RRID: AB_2064130, Abcam) and anti-Cux1 (1:200; rabbit; Cat#sc-13024, RRID: AB_2261231, Santa Cruz). The secondary antibodies used in this study were Alexa Fluor™ 488 donkey anti-rabbit (1:200; Cat#A-21206, RRID: AB_2535792, Invitrogen) and Alexa Fluor 568 donkey anti-rat (1:200; Cat#ab175475, RRID: AB_2636887, Abcam). Sections were air-dried for 30 min and treated with 10 mM citrate buffer (pH 6.0) to retrieve antigens for 1 min at 105°C in an autoclave. After cooling to RT, sections were washed with PBS and then treated with blocking solution (5% normal donkey serum, 0.1% Triton X-100 in PBS) for 1 h at RT. Then, the sections were incubated with primary antibody diluted in blocking solution for 24 h at 4°C. Next, the sections were washed in PBS and incubated with secondary antibody for 2 h at RT followed by another rinse in PBS. Sections were counterstained with DAPI (Cat#340-07971, DOJINDO) for 10 min. Finally, the sections were washed in PBS and mounted with Fluoromount™.

2.7 | Nissl staining

The brain sections were air-dried for 30 min and washed with PBS followed by incubation with 8.3×10^{-4}% toluidine blue solution (Cat#40200-30, Kanto Chemical Co., Inc.) for 10 min. After a brief rinse in PBS, the sections were washed with 95% and 100% ethanol. Then, the sections were cleared with 100% xylene for 5 seconds three times. Finally, they were mounted with Entellan new rapid mounting medium (Cat#107961, Merck) before microscopic observation.

2.8 | Whisker ablation

At P3, mice were anesthetized by hypothermia, and then their whiskers on the right were ablated using a soldering iron. At P26, mice were anesthetized with MMB by intraperitoneal injection, and perfused with PBS and PFA. After that their brains were dissected out as described in the Tissue processing section. Control mice were anesthetized by hypothermia at P3, but their whiskers were not ablated. Treated mice and control mice were from the same litter. We performed whisker ablation in the morning (10:00–11:00). Mice were fixed in the afternoon (13:00–17:00). Schematic of the time course of the whisker ablation experiment is shown in Figure 3a.

2.9 | CORT treatment

In the CORT administration experiment (P21-P31), at P21 to P31, mice were administered 0.1 mg/mL corticosterone (CORT; Cat#C0388, Tokyo Chemical Industry) in drinking water. Control mice were treated with water without CORT. At P31, these mice were perfused with PBS and PFA, and their brains were dissected out as described in the Tissue processing section. Blood samples were collected just before fixation (see the next section). In the CORT administration experiment (P1-P11), four dams nursing P1

pups were treated with CORT in their drinking water until the pups reached P11. At that time, all male pups among these dams' offspring were perfused with PBS and PFA, and their brains were dissected out as described in the Tissue processing section. The six pups with the highest blood concentrations of CORT were selected for analysis. In the control group, four dams nursing P1 pups were administered drinking water without CORT, and then all male pups among their offspring were collected at P11. In this case, each pup was assigned a random number, and the six pups with the highest numbers were selected for analysis. Mice were treated with CORT from the morning (10:00) of the first day until they were fixed in the afternoon (12:00–14:00) of the last day. Schematic of the time course of CORT administration experiment (P21-P31) is shown in Figure 4a. Schematic of the time course of CORT administration experiment (P1-P11) is shown in Figure 5a. In this study, group allocation and data collection were performed by a single person. Therefore, no blinding was performed. This study was exploratory.

2.10 | Quantification of blood concentration of CORT

Blood samples were obtained from the hearts of the CORT-treated (or control) mice just before these mice were perfused. The blood samples were transferred into 1.5-mL tubes with 10 μL of 100 mg/mL EDTA-2Na solution and mixed well by tapping. After 10 min of centrifugation (1000 g, 4°C), the supernatants were transferred into new tubes and stored at −80°C until shipping. CORT concentrations were quantified by Yanaihara Institute Inc. using a corticosterone EIA kit (Cat#YK240, Yanaihara Institute Inc.).

2.11 | Imaging analysis

Stained sections were imaged with an all-in-one fluorescence microscope (BZ-X710, Keyence).

2.12 | Quantification analysis

To examine the effect of CORT administration (P21-P31) and whisker ablation on *Hsd11b1* expression in the neocortex, we analyzed the distribution of *Hsd11b1*-positive cells in the neocortex. To create the unrolled cortical map, we set the four segments (Segments A-D: see below and Figure S3), and we measured the mediolateral spanning lengths of these four segments along with the cortical surface with ImageJ software (National Institutes of Health) in one hemisphere of each coronal section. Segment A, ranging from the ventral edge of the archicortex (dorsal peduncular, cingulate cortex, retrosplenial cortex) to the medial edge of the neocortex (M2, medial parietal association cortex, V2); Segment B, ranging from the ventral edge of the archicortex to the medial edge of the *Hsd11b1*-positive cell distribution area; Segment C, ranging from the ventral edge of the archicortex to the lateral edge of the Hsd11b1-positive cell distribution area; Segment D, the entire surface of the dorsal cortex ranging from the ventral edge of the archicortex to the dorsal edge of the paleocortex (piriform cortex, entorhinal cortex). Edges were determined by comparison between the stained sections and the Allen Brain Reference Atlas (Lein et al., 2007). Then, the lengths of the archicortex and neocortex with or without *Hsd11b1* expression were calculated as follows: length of the archicortex (length of Segment A), length of the neocortex with *Hsd11b1*-positive cells (length of Segment C − length of Segment B), and length of the neocortex without *Hsd11b1*-positive cells (length of Segment D − length of Segment C, and length of Segment B − length of Segment A). The results are shown using the horizontal cumulative bar chart (unrolled map).

Cell counting was performed by counting *Hsd11b1*-positive cells in ROIs (0.4 × 1.15 mm) set in the barrel cortex (whisker ablation) or in M1, S1, and V1 (CORT administration P1-P11). All the ROIs spanned the entire thickness of the cortex.

2.13 | Analysis of public RNAseq data

Expression of the *Hsd11b1* gene across 1691 cells isolated from adult mouse S1 was analyzed using public single-cell RNA-seq data (Zeisel et al., 2015) as previously described (Tiong et al., 2019). The annotated expression data (equivalent to the raw data in Gene Expression Omnibus (GEO, https://www.ncbi.nlm.nih.gov/geo/) with the accession GSE60361 except for the cell type annotations) were obtained from the Linnarsson laboratory website (http://linnarssonlab.org/cortex). *Hsd11b1*-expressing cells (expression score >0) in each of the six Level-1 classes (astrocytes, endothelial cells, interneurons, microglia, oligodendrocytes, and pyramidal neurons) were plotted according to their expression score.

2.14 | Statistical analyses

In the whisker ablation experiment (Figure 3b) and CORT administration experiment (P21-P31) (Figure 4b), data are expressed as the mean ± SEM. In the whisker ablation experiment (Figure 3c), CORT administration experiment (P1-P11) (Figure 5b), retrograde tracing experiment (Figure S1c), and blood CORT concentration measurements (Figures S4 and S5), data are presented as box-and-whisker plots with individual data points. An outlier was defined as the datapoint beyond 1.5× the interquartile range. In Figure S5, the filled data points in red are used for cell counting, while an outlier is shown as an open red point. The centerline represents the median; the edges of the box are the first and third quartiles; the whiskers are 1.5× the interquartile range; cross marks, average. The normality of our data was evaluated by the Shapiro–Wilk test. We could not verify the normality of our data; thus, all data were analyzed using the non-parametric Wilcoxon rank sum test. In the CORT administration experiment (P1-P11), an outlier was excluded (Figure 5b), but the full data set (including the outlier) was also visualized (Figure S6). In the

preliminary CORT administration experiment (P1-P11) using three animals in each group, the power and effect size calculated based on the results were 0.63 and 2.6 respectively. Therefore, we set the expected effect size for this CORT administration experiment as 2. We determined sample size as 6, since 6 satisfied the statistical convention (power: 0.8, α error probability: 0.05). For calculation of effect size and sample size, we used G*power 3.1 (Faul et al., 2009; https://www.psychologie.hhu.de/arbeitsgruppen/allgemeine-psychologie-und-arbeitspsychologie/gpower). Significance was defined as $p < 0.05$. JMP® 14 (SAS Institute Inc.) was used for statistical analysis. Full statistical reports are shown in Tables S1-S4.

Custom-made materials will be shared upon reasonable request.

3 | RESULTS

3.1 | *Hsd11b1*-positive cells were distributed primarily in S1 of the adult mouse neocortex

Since the tangential distribution pattern of *Hsd11b1*-positive cells remains elusive, we examined *Hsd11b1* expression in the cortex with ISH on coronal sections of the adult mouse brain (Figure 1). *Hsd11b1*-positive cells were detected as a thin band primarily in S1 (Figure 1c–l). The areas directly neighboring S1 contained infrequent positive cells, and no positive cells were found in other areas of the neocortex. Within the archicortex, *Hsd11b1*-positive cells were detected in the retrosplenial cortex (Figure 1h–m). In the adult mouse, most *Hsd11b1*-positive cells were morphologically pyramidal neurons according to the Nissl staining data (Figure 2B, k–k′′). Here, we used three mice. Our retrograde tracer injection experiments showed that the ratio of *Hsd11b1*-positive cells in the S1 neurons projecting to ipsilateral M1 was 26.9 ± 1.6%, whereas that to the contralateral S1 was 15.8 ± 1.5% (Figure S1a–c). In this experiment, we used three mice. These results indicated that *Hsd11b1*-positive cells contained excitatory neurons. Our analysis of a public single-cell RNA-seq data set also indicated that *Hsd11b1* is expressed in some pyramidal neurons.

3.2 | Distribution pattern of *Hsd11b1*-positive cortical cells dynamically changed during postnatal development

We next asked whether the expression pattern described above was maintained from the early developmental stage or gradually shaped during development. We profiled the distribution pattern of *Hsd11b1*-positive cells in the three primary cortices at multiple postnatal stages (P0, P3, P4, P6, P8, P14, P17, P26, and P56) by ISH (three mice for each stage). We found a dynamic change in the gross distribution pattern of *Hsd11b1*-positive cells: cells at P0 were rather specifically localized in S1, then a gradual expansion covering the entire neocortex was observed and peaking at P8, followed by re-restriction down to S1 and the retrosplenial cortex at P56 (Figure 2A). We also investigated the distribution pattern in M1, S1, and V1 (Figures 2B, S2). To identify the layer that contained *Hsd11b1*-positive cells, we performed Nissl staining and IHC on adjacent sections with antibodies against Cux1 and Ctip2 as markers for layers 2–4 and layer 5, respectively. At P0, *Hsd11b1*-positive cells were detected only in S1 among the three areas (Figure 2B, b). These cells in S1 were distributed from the deeper region of layer 4 to layer 5 (Figure 2B, b–b′′). Faint expression of *Hsd11b1* was observed broadly in a radial manner around these cells (Figure 2B, b). At P3, the laminar distribution of *Hsd11b1*-positive cells in S1 (Figure 2B, e) became broader than that at P0 (Figure 2B, b). A number of discrete cells with high expression was seen within the broad *Hsd11b1* expression area (Figure 2B, e). In addition, we also observed broad expression and discrete cells with high expression in the same layers in V1 (Figure 2B, f–f′). At P8, in S1, the discrete cells with high expression were largely confined within layer 5 (Figure 2B, h–h′′), while there was no notable change in the broadness of the expression layers compared to P3 (Figure 2B, e–e′′). The expression pattern in V1 (Figure 2B, i–i′′) did not show obvious differences from that at P3 (Figure 2B, f–f′′). At this stage, in M1, both radially broad expression and discrete cells were observed (Figure 2B, g). At P26 and P56, *Hsd11b1*-positive cells were not observed in M1 and V1 (Figure 2B, j, Figure 2B, l, Figure S2h, i, z, aa), while still observed in S1 (Figure 2B, k, Figure S2q, r). Interestingly, only discrete cells with high expression were mostly confined within layer 5 (Figure 2B, k–k′′, Figure S2q–q′′, r–r′′). Overall, the *Hsd11b1* expression pattern dynamically changed during postnatal development and stabilized to a restricted pattern of expression in layer 5 of S1 after P26.

3.3 | *Hsd11b1*-positive cell distribution did not depend on sensory inputs

We asked what shape the expression pattern of *Hsd11b1* in the cortex. We examined whether stable *Hsd11b1* expression in S1 after P26 depends on sensory input. The somatosensory information from one side of the animal is conveyed to S1 on the contralateral hemisphere of the cortex (Fenlon et al., 2017). Therefore, if sensory input affects the expression of *Hsd11b1* in S1, blocking sensory input unilaterally would cause distribution changes in the contralateral hemisphere but not in the ipsilateral hemisphere. Within S1, we focused on the barrel cortex that receives sensory information detected by whiskers (Petersen, 2007). We ablated the whiskers on the right side of three mice by cauterization at P3 and then examined whether the distribution of *Hsd11b1*-positive cells in the neocortex was altered at P26 by ISH (Figure 3a).

First, we measured the mediolateral spanning lengths of the *Hsd11b1*-expressing region along the cortical surface of the cortex in coronal sections, including the barrel cortex. To define and describe the *Hsd11b1* expression region precisely, we set the four segments (Figure S3a). We presented this result as an unrolled map (Figure 3b, Figure S3B). There was no significant difference in the mediolateral spanning lengths of the *Hsd11b1*-expressing regions between

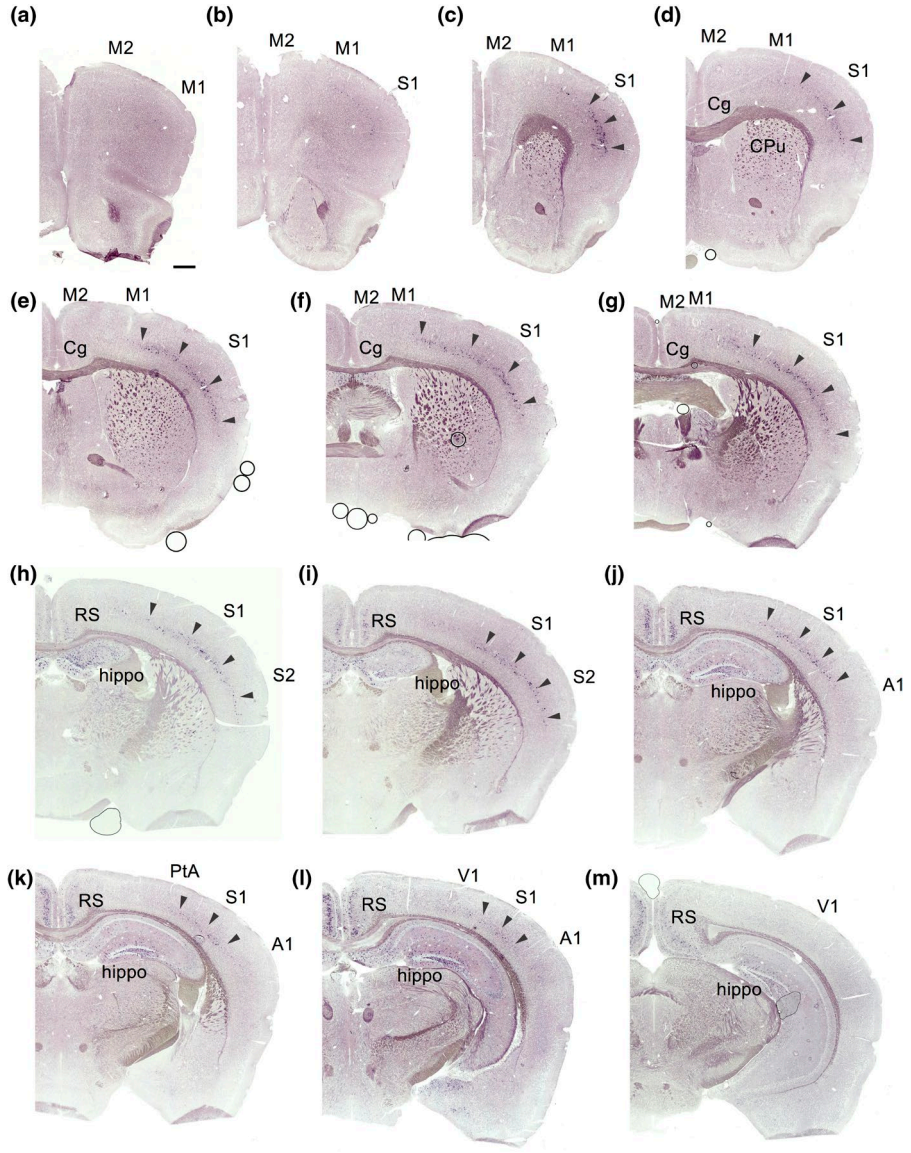

FIGURE 1 *Hsd11b1* was expressed in limited cortical areas in adult mice. *Hsd11b1* mRNA expression was examined by ISH using coronal sections of the adult (P56) mouse cerebral cortices (a–m). Sections that cover the full rostrocaudal range of *Hsd11b1* expression in S1 are shown. (a) is the most rostral and (m) is the most caudal. (c–l) *Hsd11b1* expression was detected as a band in S1 and S2. The *Hsd11b1*-expressing regions in the neocortex are indicated with arrowheads. (h–m) *Hsd11b1* expression was also detected in the hippocampus (hippo) and the retrosplenial cortex (RS). Scale bar, 500 μm. $N = 3$ mice. The representative images are shown. (d) and (i) are flipped horizontally from the original images

the two hemispheres. We next counted the numbers of *Hsd11b1*-positive cells in the ROIs set in the barrel cortex. We found no difference in the numbers between the ipsi- and contralateral barrel cortices (Figure 3c). These results suggest that the distribution pattern and density of *Hsd11b1*-positive cells in S1 do not depend on sensory inputs.

FIGURE 2 The distribution pattern of *Hsd11b1*-positive cells dynamically changed during postnatal development. (A) Coronal sections at the S1 level of mice at four postnatal stages (P0, P3, P8, and P56). *Hsd11b1* expression was examined by ISH. The *Hsd11b1*-expressing regions in the neocortex are indicated with arrowheads. The distribution of *Hsd11b1*-positive cells dynamically changed with development, especially in the neocortex. Scale bar, 500 μm. The original image of panel A "P56" is identical to that of Figure 1j. (B) (a-l) Higher magnification views of the three primary cortical areas (M1, S1, and V1) in the neocortex of the same animals in (A). The cortical layers are shown (L1, layer 1; L2/3, layer 2/3; L4, layer 4; L5, layer 5; and L6, layer 6). The inset in (b) shows the higher magnification image of the boxed area. Scale bar in the inset, 50 μm. (a'-l') IHC with antibodies against Cux1 (layer 2–4 marker) and Ctip2 (layer 5 marker) on the adjacent sections of (a-l). (a''–l'') Nissl staining on the adjacent sections of (a-l). Dotted lines, the borders between the neocortex and the white matter. Scale bar, 100 μm. $N = 3$ mice. Medial is to the left, lateral is to the right. Panels of all analyzed developmental stages are shown in Figure S2

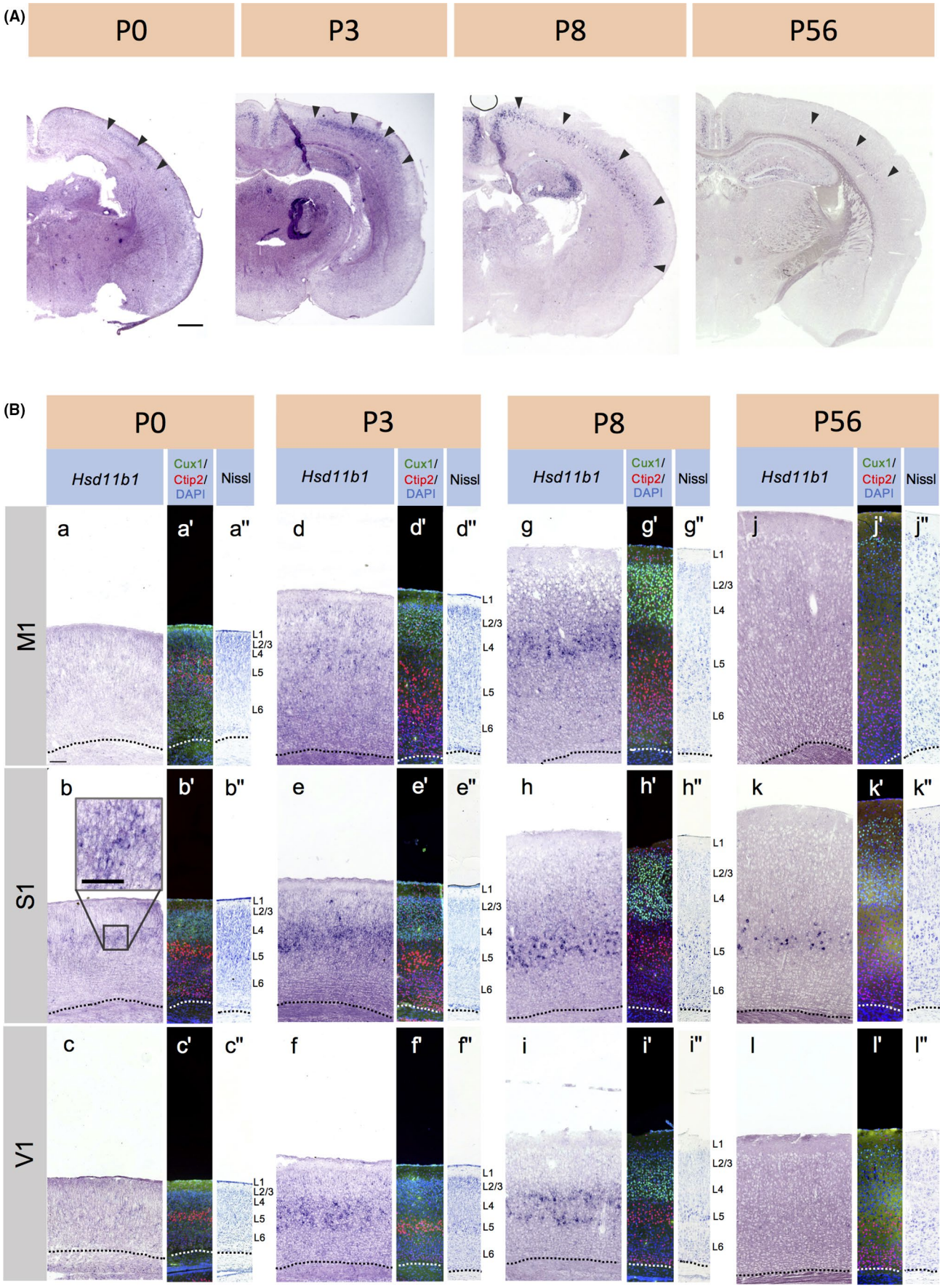
(A)
P0
P3
P8
P56
(B)
P0
P3
P8
P56
Hsd11b1
Cux1/ Ctip2/ DAPI
Nissl
M1
S1
V1
a
a'
a"
b
b'
b"
c
c'
c"
d
d'
d"
e
e'
e"
f
f'
f"
g
g'
g"
h
h'
h"
i
i'
i"
j
j'
j"
k
k'
k"
l
l'
l"
L1
L2/3
L4
L5
L6

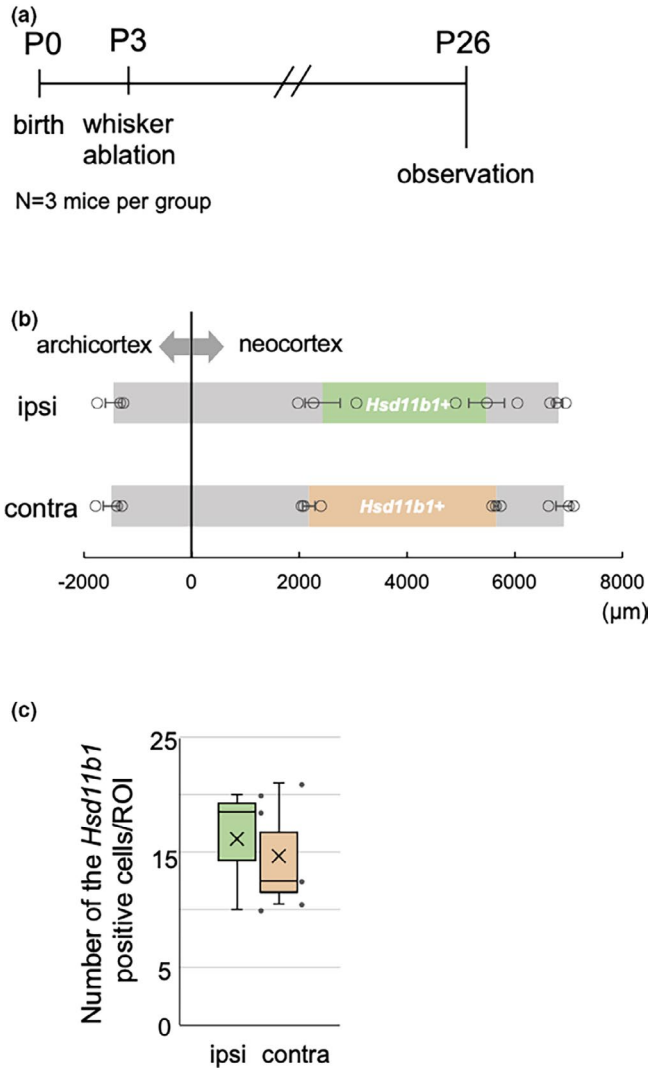

FIGURE 3 Sensory input did not affect the tangential distribution pattern or density of *Hsd11b1*-positive cells in the barrel cortex. We ablated whiskers on the right side of the snout at P3 and examined the expression pattern of *Hsd11b1* by ISH at P26 in the cortex. (a) Schematic of the time course of the whisker ablation experiment. (b) Unrolled maps of the cortices ipsilateral and contralateral to the whisker-ablated side show the *Hsd11b1* expression areas in the coronal sections containing the barrel cortex. In each bar, green and light brown parts show the distribution areas of *Hsd11b1*-positive cells. The gray parts show the archicortex and neocortex without *Hsd11b1*-positive cells. These data are mean ± SEM; $N = 3$ mice. The data were analyzed using the Wilcoxon rank sum test. Full statistical reports are shown in Table S1. (c) Quantification of the number of *Hsd11b1*-positive cells in the ROIs set in the barrel cortices ipsilateral (green) and contralateral (light brown) to the whisker-ablated side. Data are presented as box-and-whisker plots with individual data points. Centerline, median; box edges, upper and lower quartiles including median; whiskers, 1.5× interquartile range; cross marks, average. $N = 3$ mice. The data were analyzed using the Wilcoxon rank sum test. Full statistical reports are shown in Table S1

3.4 | CORT administration for 10 days from P21 had no effect on the distribution pattern of *Hsd11b1*-positive cells

Hsd11b1 encodes 11β-HSD1, which controls the local activation of CORT (Seckl & Walker, 2001; Yau & Seckl, 2012). Thus, we examined the relationship between CORT and *Hsd11b1*-positive cells in the cortex. We tested whether an increase in blood CORT levels affected the expression of *Hsd11b1* in cortical cells since *Hsd11b1* is under the control of CORT via glucocorticoid-responsive elements (GREs) in humans (Inder et al., 2012). We administered CORT in drinking water to the mice for 10 days from P21 onwards and observed the distribution pattern of *Hsd11b1*-positive cells by ISH at P31 (Figure 4a). An increase in the blood concentration of CORT was confirmed in the CORT-treated group (Figure S4). Here, we concluded that there was no difference between these two groups (three mice per group) in the distribution pattern of the *Hsd11b1*-expressing region (Figure 4b).

3.5 | CORT administration at the early postnatal stage affected the number of *Hsd11b1*-positive cells in the cortex

Next, we asked whether high blood levels of CORT affect the dynamic expression profile during early development. We examined the effects of CORT administration for 10 days from P1 on the distribution of *Hsd11b1*-positive cells at P11 (Figure 5a). We administered CORT to nursing dams to increase the systemic CORT level of their pups (CORT-treated group). Statistically, an increase in the blood concentration of CORT was confirmed in the CORT-treated group (12 pups per group) (Figure S5). In detail, increases in the blood concentration of CORT were observed only in six pups of CORT-treated group. In the other six pups in the CORT-treated group, the blood concentrations of CORT were comparable with those of the control group. There was an outlier that is over 1.5× the interquartile range, of which systemic CORT level was too high, in the former six pups of the CORT-treated group. To study the correlation between systemic CORT level and expression of *Hsd11b1*, we selected five pups (excluding the outlier) with the highest blood concentrations of CORT for further cell counting. Since *Hsd11b1*-positive cells were distributed widely throughout the cortex, we evaluated the effects by counting the number of *Hsd11b1*-positive cells in the regions of interest (ROIs) set in three areas (M1, S1, and V1) (Figure 5b). In all regions, the number of *Hsd11b1*-positive cells was significantly decreased in the CORT-treated group compared with the control group (Figure 5b). We also showed the data including the outlier as Figure S6. These results suggest that high blood levels of CORT in the early postnatal stage decrease the number of *Hsd11b1*-positive cells at P11.

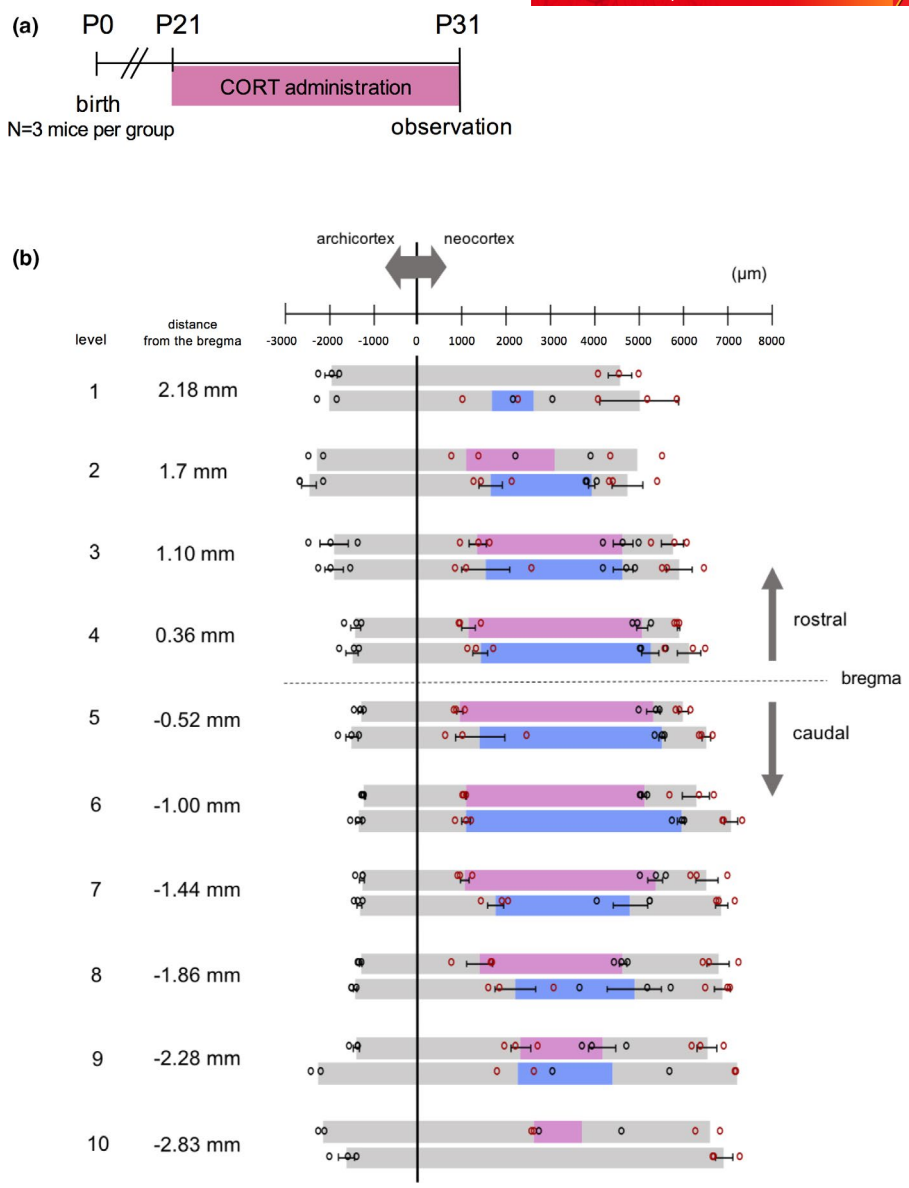

FIGURE 4 Tangential distribution pattern of *Hsd11b1*-positive cells with CORT administration from P21 to P31. (a) Schematic of the time course of CORT administration. (b) Unrolled maps of the cortex show the *Hsd11b1* expression area at 10 rostrocaudal levels represented as cumulative bar graphs of length along the cortical surface of coronal sections. The bregma level is shown with the dotted line. In each bar, the pink and blue bars show the distribution areas of *Hsd11b1*-positive cells in CORT-treated and control mice. The gray parts show the archicortex and the neocortex without *Hsd11b1*-positive cells. The data are mean ± SEM; $N = 3$ mice for each group. In the bars without error bars, the sections with *Hsd11b1*-positive cells were not enough to calculate SEM. The average distance from bregma at each level and the ranges are as follows: level 1, 2.18 mm (2.34-2.10 mm); level 2, 1.70 mm (1.94-1.54 mm); level 3, 1.10 mm (1.18-0.98 mm); level 4, 0.36 mm (0.62-0.14 mm); level 5, -0.52 mm (-0.46 to -0.70); level 6, -1.00 mm (-0.94 to -1.06 mm); level 7, -1.44 mm (-1.34 to -1.58 mm); level 8, -1.86 mm (-1.70 to -1.94 mm); level 9, -2.28 mm (-2.18 to -2.46 mm); and level 10, -2.83 mm (-2.70 to -3.08 mm). The data were analyzed using the Wilcoxon rank sum test. Full statistical reports are shown in Table S2

4 | DISCUSSION

In this study, we demonstrated that the *Hsd11b1* expression pattern changed dynamically in the developing neocortex. At P0, *Hsd11b1* expression was observed only in S1. The area where expression was observed gradually expanded from P3 and then reached a peak around P8 to P14. After that, the areas of ISH-positive cells gradually narrowed and finally settled in layer 5 of S1 after P26. The period when the *Hsd11b1*-expressing region expanded (P3-P14) overlapped with the critical period of synaptic or structural plasticity in the neocortex. Additionally, the peak term of *Hsd11b1* expression almost coincides with the period when synapse formation induced by microglia occurs (P8-P10) (Miyamoto et al., 2016). It is also known that microglial proliferation is induced by CORT (Nair & Bonneau, 2006) and dendritic spine pruning is induced by chronic high CORT (Moda-Sava et al., 2019). Based on these observations, it is likely that the local CORT regulated by the effect of 11β-HSD1 is involved in normal circuit formation in the developing neocortex, possibly by controlling the number of microglia.

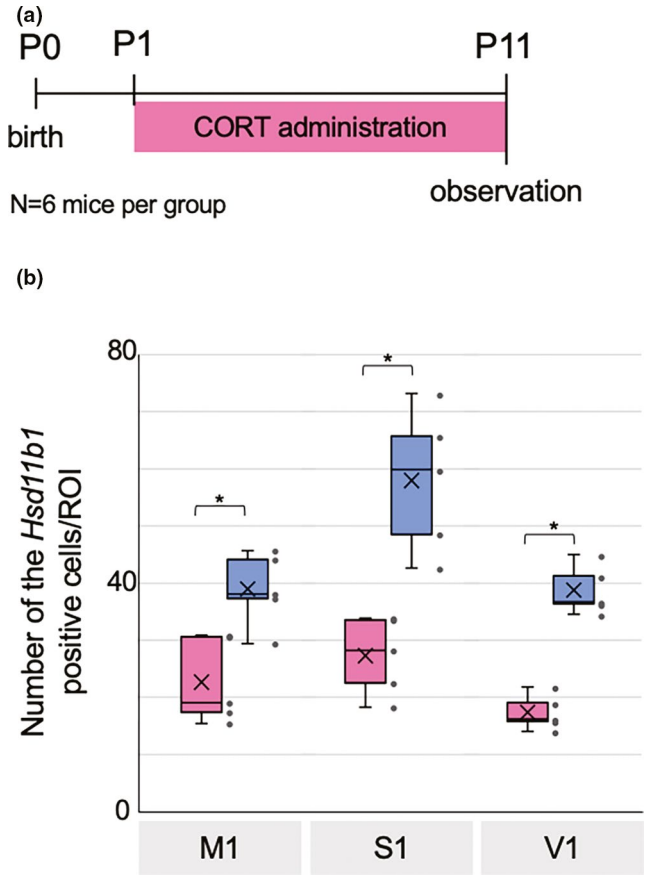

FIGURE 5 The number of *Hsd11b1*-positive cells was decreased by CORT administration to the nursing dams from P1 to P11. (a) Schematic of the time course of CORT administration to the nursing dams. (b) Quantification of the numbers of *Hsd11b1*-positive cells in the ROIs set in three primary cortical areas (M1, S1, and V1). The pink and blue bars show data from the CORT-treated and control mouse groups. An outlier is excluded (In Figure S6, the full data set was also visualized). Data are presented as box-and-whisker plots with individual data points. Centerline, median; box edges, upper and lower quartiles including median; whiskers, 1.5× interquartile range; cross marks, average. $N = 6$ mice for each group. Asterisks show significant differences with $p < 0.05$. The data were analyzed using the Wilcoxon rank sum test. Full statistical reports are shown in Table S3. We performed post hoc power analysis and confirmed that the power of each test was over 0.8 (M1: 0.98, S1: 0.99, V1: 1.00)

Our observation of a transient increase in *Hsd11b1* expression suggests that the developing neocortex, especially at approximately P8 to P14, may need the higher local concentration of CORT than the systemic level. In the CORT administration experiment during early postnatal development, we observed reduced numbers of *Hsd11b1*-positive cells compared with the control at P11 when expanded expression regions were observed in the neocortex. Therefore, there is possibly a mechanism that adjusts the local CORT concentration to the situation and prevents it from overshooting. In addition, our observations indicate that stress in nursing dams potentially influences the development of the pups' brains through 11β-HSD1.

The expression of *Hsd11b1* is known to be regulated by two specific promoters, known as the P1 and P2 promoters. Furthermore, *Hsd11b1* transcription regulators, including CCAAT/enhancer-binding protein beta (C/EBPβ), peroxisome proliferator-activated receptors (PPARs), and tumor necrosis factor α (TNF-α), have been reported in mice (Chapman et al., 2013). The mechanism of 11β-HSD1 activity regulation varies from organ to organ (Bruley et al., 2006). Thus, it will be important for future studies to reveal the exact mechanisms of 11β-HSD1 activity regulation in the developing mouse neocortex.

Recently, it has been increasingly recognized that early-life stress affects neural circuits and brain function. For example, in mice, stress caused by maternal separation before weaning induces hypersensitivity in adults (Takatsuru et al., 2009). In humans, higher stress-related hormone levels at 4 years old are correlated with lower connectivity between the prefrontal cortex and amygdala at 18 years old (Burghy et al., 2012). Here, we identified the *Hsd11b1* gene as one of the molecular entitles that changes its expression in the developing neocortex, depending on the level of the stress hormone during early postnatal development. It is also known that 11β-HSD1 affects brain function. A preceding study shows that 11β-HSD1$^{-/-}$ mice resisted the memory impairment induced by stress and aging, and the authors concluded that hippocampal CORT generated by 11β-HSD1, which increases with aging, impairs spatial memory in aged mice (Yau et al., 2015). Our results should be a key to revealing the relationship between neonatal stress, particularly reflecting those on mothers, and its effects on neocortical development/functions via local hormonal regulation.

ACKNOWLEDGMENTS

We thank T. Iguchi and M. Yasumura for helpful discussion, S. Y. X. Tiong for critical reading, T. Yamamoto for advice on statistical analyses, and M. Yamaguchi, Y. Shibuya, A. Yoshinori, and K. Danke for secretarial assistance. Animal experiments were supported by The Institute of Experimental Animal Science, Faculty of Medicine, Osaka University. The imaging experiments were supported by the Center for Medical Research and Education, Graduate School of Medicine, Osaka University. This work was supported in part by grants from Takeda Science Foundation, NOVARTIS Foundation (Japan) for the Promotion of Science, Naito Foundation, and JSPS KAKENHI (Grant numbers JP26830027, and JP17K07076 (to Y.O.) and JP15K15015, JP25293043, JP17H04014, and 20H03414 (to M.S.)). We declare no conflict of interest.

AUTHOR CONTRIBUTIONS

M. Doi; Conception and design, collection and assembly of data, data analysis and interpretation, manuscript writing, final approval of manuscript. Y. Oka; Financial support, conception and design, data analysis and interpretation, manuscript writing, final approval of manuscript. M. Taniguchi; Some part of histological studies, final approval of manuscript. M. Sato; Financial support, conception and design, data analysis and interpretation, manuscript writing, final approval of manuscript.

ORCID

Yuichiro Oka https://orcid.org/0000-0003-0543-3297
Makoto Sato https://orcid.org/0000-0002-6805-8351

REFERENCES

Andrew, R., Westerbacka, J., Wahren, J., Yki-Järvinen, H., & Walker, B. E. (2005). The contribution of visceral adipose tissue to splanchnic cortisol production in healthy humans. *Diabetes*, 54, 1364–1370. https://doi.org/10.2337/diabetes.54.5.1364.

Bruley, C., Lyons, V., Worsley, A. G. F., Wilde, M. D., Darlington, G. D., Morton, N. M., Seckl, J. R., & Chapman, K. E. (2006). A novel promoter for the 11β-hydroxysteroid dehydrogenase type 1 gene is active in lung and is C/EBPα independent. *Endocrinology*, 147, 2879–2885. https://doi.org/10.1210/en.2005-1621.

Burghy, C. A., Stodola, D. E., Ruttle, P. L., Molloy, E. K., Armstrong, J. M., Oler, J. A., & Fox, M. E. (2012). Developmental pathways to amygdala-prefrontal function and internalizing symptoms in adolescence. *Nature Neuroscience*, 15, 1736–1741. https://doi.org/10.1038/nn.3257.

Chapman, K., Holmes, M., & Seckl, J. (2013). 11β-hydroxysteroid dehydrogenases intracellular gate-keepers of tissue glucocorticoid action. *Physiological Reviews*, 93, 1139–1206. https://doi.org/10.1152/physrev.00020.2012.

Diamond, D. M., Bennett, M. C., Fleshner, M., & Rose, G. M. (1992). Inverted-U relationship between the level of peripheral corticosterone and the magnitude of hippocampal primed burst potentiation. *Hippocampus*, 2, 421–430. https://doi.org/10.1002/hipo.450020409.

Faul, F., Erdfelder, E., Buchner, A., & Lang, A.-G. (2009). Statistical power analyses using G*Power 3.1: Tests for correlation and regression analyses. *Behavior Research Methods*, 41, 149–1160. https://doi.org/10.3758/BRM.41.4.1149.

Fenlon, L. R., Suárez, R., & Richards, L. J. (2017). The anatomy, organisation and development of contralateral callosal projections of the mouse somatosensory cortex. *Brain Neuroscience Advances*, 1, 1–9. https://doi.org/10.1177/2398212817694888.

Funder, J. W. (1997). Glucocorticoid and mineralocorticoid receptors: Biology and clinical relevance. *Annual Review of Medicine*, 48, 231–240. https://doi.org/10.1146/annurev.med.48.1.231.

Holmes, M. C., Carter, R. N., Noble, J., Chitnis, S., Dutia, A., Paterson, J. M., Mullins, J. J., Seckl, J. R., & Yau, J. L. W. (2010). 11β-Hydroxysteroid dehydrogenase type 1 expression is increased in the aged mouse hippocampus and parietal cortex and causes memory impairments. *Journal of Neuroscience*, 30, 6916–6920. https://doi.org/10.1523/JNEUROSCI.0731-10.2010.

Inder, W. J., Obeyesekere, V. R., Jang, C., & Saffery, R. (2012). Evidence for transcript-specific epigenetic regulation of glucocorticoid-stimulated skeletal muscle 11β-hydroxysteroid dehydrogenase-1 activity in type 2 diabetes. *Clinical Epigenetics*, 4, 24. https://doi.org/10.1186/1868-7083-4-24.

Lein, E. S., Hawrylycz, M. J., Ao, N., Ayres, M., Bensinger, A., Bernard, A., Boe, A. F., Boguski, M. S., Brockway, K. S., Byrnes, E. J., Chen, L., Chen, L. I., Chen, T.-M., Chi Chin, M., Chong, J., Crook, B. E., Czaplinska, A., Dang, C. N., Datta, S., … Jones, A. R. (2007). Genome-wide atlas of gene expression in the adult mouse brain. *Nature*, 445, 168–176. https://doi.org/10.1038/nature05453.

Macrì, S., Granstrem, O., Shumilina, M., Gomes, A., dos Santos, F. J., Berry, A., Saso, L., & Laviola, G. (2009). Resilience and vulnerability are dose-dependently related to neonatal stressors in mice. *Hormones and Behavior*, 56, 391–398. https://doi.org/10.1016/j.yhbeh.2009.07.006.

Miyamoto, A., Wake, H., Ishikawa, A. W., Eto, K., Shibata, K., Murakoshi, H., Koizumi, S., Moorhouse, A. J., Yoshimura, Y., & Nabekura, J. (2016). Microglia contact induces synapse formation in developing somatosensory cortex. *Nature Communications*, 7, 12540. https://doi.org/10.1038/ncomms12540.

Moda-Sava, R. N., Murdock, M. H., Parekh, P. K., Fetcho, R. N., Huang, B. S., Huynh, T. N., & Witztum, J. (2019). Sustained rescue of prefrontal circuit dysfunction by antidepressant-induced spine formation. *Science*, 364, 6436. https://www.science.org/doi/10.1126/science.aat8078.

Nair, A., & Bonneau, R. H. (2006). Stress-induced elevation of glucocorticoids increases microglia proliferation through NMDA receptor activation. *Journal of Neuroimmunology*, 171, 72–85. https://doi.org/10.1016/j.jneuroim.2005.09.012.

Pedrazzoli, M., Losurdo, M., Paolone, G., Medelin, M., Jaupaj, L., Cisterna, B., Slanzi, A., Malatesta, M., Coco, S., & Buffelli, M. (2019). Glucocorticoid receptors modulate dendritic spine plasticity and microglia activity in an animal model of Alzheimer's disease. *Neurobiology of Diseases*, 132, 104568. https://doi.org/10.1016/j.nbd.2019.104568.

Petersen, C. C. H. (2007). The functional organization of the barrel cortex. *Neuron*, 56, 339–355. https://doi.org/10.1016/j.neuron.2007.09.017.

Sandeep, T. C., & Walker, B. R. (2001). Pathophysiology of modulation of local glucocorticoid levels by 11 β-hydroxysteroid dehydrogenases. *Trends in Endocrinology and Metabolism*, 12, 446–453. https://doi.org/10.1016/S1043-2760(01)00499-4.

Scorrano, F., Carrasco, J., Pastor-Ciurana, J., Belda, X., Rami-Bastante, A., Bacci, M. L., & Armario, A. (2015). Validation of the long-term assessment of hypothalamic-pituitary-adrenal activity in rats using hair corticosterone as a biomarker. *The FASEB Journal*, 29, 859–867. https://doi.org/10.1096/fj.14-254474.

Seckl, J. R. (1997). 11β-Hydroxysteroid dehydrogenase in the brain: A novel regulator of glucocorticoid action? *Frontiers in Neuroendocrinology*, 18, 49–99. https://doi.org/10.1006/frne.1996.0143.

Seckl, J. R., & Walker, B. R. (2001). 11βHSD Type I - A tissue-specific amplifier of glucocorticoid action. *Endocrinology*, 142, 1371–1376. https://doi.org/10.1210/endo.142.4.8114.

Takatsuru, Y., Yoshitomo, M., Nemoto, T., Eto, K., & Nabekura, J. (2009). Maternal separation decreases the stability of mushroom spines in adult mice somatosensory cortex. *Brain Research*, 1294, 45–51. https://doi.org/10.1016/j.brainres.2009.07.092.

Tiong, S. Y. X., Oka, Y., Sasaki, T., Taniguchi, M., Doi, M., Akiyama, H., & Sato, M. (2019). *Kcnab1* is expressed in subplate neurons with unilateral long-range inter-areal projections. *Frontiers in Neuroanatomy*, 13, 1–16. https://doi.org/10.3389/fnana.2019.00039.

Yau, J. L. W., McNair, K. M., Noble, J., Brownstein, D., Hibberd, C., Morton, N., Mullins, J. J., Morris, R. G. M., Cobb, S., & Seckl, J. R. (2007). Enhanced hippocampal long-term potentiation and spatial learning in aged 11β-hydroxysteroid dehydrogenase type 1 knockout mice. *Journal of Neuroscience*, 27, 10487–10496. https://doi.org/10.1523/JNEUROSCI.2190-07.2007.

Yau, J. L. W., & Seckl, J. R. (2012). Local amplification of glucocorticoids in the aging brain and impaired spatial memory. *Frontiers in Aging Neuroscience*, 4, 1–15. https://doi.org/10.3389/fnagi.2012.00024.

Yau, J. L. W., Wheelan, N., Noble, J., Walker, B. R., Webster, S. P., Kenyon, C. J., Ludwig, M., & Seckl, J. R. (2015). Intrahippocampal glucocorticoids generated by 11β-HSD1 affect memory in aged mice. *Neurobiology of Aging*, 36, 334–343. https://doi.org/10.1016/j.neurobiolaging.2014.07.007.

Zeisel, A., Munoz-Manchado, A. B., Codeluppi, S., Lonnerberg, P., La Manno, G., Jureus, A., Marques, S., Munguba, H., He, L., Betsholtz, C., Rolny, C., Castelo-Branco, G., Hjerling-Leffler, J., & Linnarsson, S. (2015). Cell types in the mouse cortex and hippocampus revealed by single-cell RNA-seq. *Science*, 347, 1138–1141. https://doi.org/10.1126/science.aaa1934.

SUPPORTING INFORMATION

Additional supporting information may be found in the online version of the article at the publisher's website.

How to cite this article: Doi, M., Oka, Y., Taniguchi, M., & Sato, M. (2021). Transient expansion of the expression region of *Hsd11b1*, encoding 11β-hydroxysteroid dehydrogenase type 1, in the developing mouse neocortex. *Journal of Neurochemistry*, 00, 1–11. https://doi.org/10.1111/jnc.15505